Research Article

A simple low cost method for synthesis of SnO$_2$ nanoparticles and its characterization

Shaheen Naz[1,2] · Iqra Javid[1,2] · Subhrajit Konwar[2] · Karan Surana[2] · Pramod K. Singh[2] · Mohit Sahni[2] ·
Bhaskar Bhattacharya[2,3]

Abstract
Nanomaterials have gained a lot of interest due to their application in various fields. Tin oxide (SnO$_2$) is an important n-type wide band-gap semiconductor in the field of gas sensing devices due to its chemical and mechanical stability. Here, SnO$_2$ nanoparticles were synthesized by a simple chemical co-precipitation method followed by annealing the obtained nanoparticles at different temperatures. Several characterization techniques like powder X-ray Diffraction, Scanning Electron Microscope, Energy-Dispersive X-Ray spectroscopy, and Ultraviolet–Visible spectroscopy, Fourier Transform Infrared Spectroscopy were carried out to analyze the structure, size, morphology, elemental composition and optical properties of the prepared SnO$_2$ nanoparticles.

Keywords Tin oxide · Nanoparticles · Chemical co-precipitation · Bandgap

1 Introduction

Nanomaterials have attracted the interest of scientists all across the globe after the famous inspiring speech by Feynman stating, 'there is plenty of room at the bottom' [1]. This ignited a revolution in the research community which led to exploration of materials and their properties down to the nano scale in every field of science. Nanoparticles of wide-bandgap semiconductors such as Tin Oxide (SnO$_2$) have been in the limelight as they have found applications in gas sensing, humidity and temperature sensing, lithium batteries, transistors, transparent conducting electrodes, liquid crystal displays, photovoltaic devices and as a key element in opto-electronic devices [2–9]. The performance of such semiconducting nanoparticles like their response time, stability, selectivity, sensitivity etc. depends chiefly upon the size of particles, which in turn can be controlled by varying the pH of the solution, concentration of

precursor and precipitating reagents [3, 4]. SnO$_2$ is a versatile n-type semiconductor with a crystalline structure and depending on the synthesis procedure it can have optical (direct) transition corresponding to 3.6–3.8 eV or an indirect transition near 2.7–3.1 eV [5, 6].

SnO$_2$ can be synthesized by various methods like crystal spray pyrolysis, hydrothermal methods, thermal evaporation, microwave-assisted combustion method, sol–gel method and electrochemical synthesis as mentioned in previous literatures [5–13]. Koshay et al. had prepared the nanoparticles through sol–gel technique having a tetragonal structure with an average particle size of 12.10 nm [2]. Naje et al. conducted experiments to obtain SnO$_2$ nanoparticles through chemical precipitation method. The morphology shows tetragonal structure with particle size in the range of 8–10 nm [6]. Razeghizadeh et al. performed the experiments with Sol–Gel technique which results in tetragonal structure of SnO$_2$ having different average

✉ Bhaskar Bhattacharya, bhaskar.phys@bhu.ac.in | [1]Department of Electronics and Communication Engineering, School of Engineering and Technology, Sharda University, Greater Noida, U.P. 201310, India. [2]Material Research Laboratory, School of Basic Sciences and Research, Sharda University, Greater Noida, U.P. 201310, India. [3]Department of Physics, MMV, Banaras Hindu University, Varanasi, U.P. 221005, India.

crystallite size for different solution concentrations (17 nm, 18.8 nm, 74.8 nm for 0.1, 0.3, 0.5 M respectively) [7]. Thakre et al. made SnO₂ thin solid films through physical vapour deposition technique. Further the thin films were used for gas sensing purpose [9]. Nehru et al. synthesized the SnO₂ nanopowder through microwave assisted combustion method and tetragonal rutile structure with 8 nm particle size was found [12]. Chen et al. had synthesized the tin oxide nanoparticles through electrochemical synthesis having tetragonal rutile structure and the average size of the annealed particles was found to be 15.4, 12.5, 11.8 nm for different voltages i.e. 20 V, 30 V and 40 V respectively [14].

Amongst the various proposed methods, chemical co-precipitation method possesses the advantages of being easily reproducible, utilizes simple laboratory equipment, low in impurity, less time consuming, and ease of processability. Hence in this paper, chemical co-precipitation method has been chosen for synthesis of SnO₂ nanoparticles (NPs) [15]. The prepared SnO₂ NPs were annealed at three different temperatures. The finally obtained NPs were analyzed for their structure, size, morphology, elemental composition and optical properties by several characterization techniques like powder X-ray Diffraction (XRD), Scanning Electron Microscope (SEM), Energy-Dispersive X-Ray spectroscopy (EDX), Fourier Transform Infrared (FTIR) Spectroscopy, and Ultraviolet–Visible (UV) spectroscopy. XRD confirmed the tetragonal structure of the NPs and the average crystallite size increased with the rise in annealing temperature which led to change in the bandgap.

2 Materials

The chemicals were used as received without any additional purification. Stannous chloride (SnCl₂·2H₂O) was purchased from Central drug house (p) Ltd. having molecular weight 225.63 (99.6% pure). Ethanol was purchased from Changshu Hongsheng fine chemicals. Liquor Ammonia (NH₃) and Hydrochloric acid (HCl) were purchased from Fisher Scientific. Double Distilled (DD) water prepared in laboratory was used wherever necessary.

3 Synthesis

SnO₂ NPs were prepared by chemical co-precipitation method. 0.27 M SnCl₂·2H₂O was added to DD water and ethanol (2.2:1 v/v) in a 1000 mL beaker under continuous magnetic stirring for 60 min in order to obtain a homogeneous solution. 50 mL of HCl was added drop wise in order to reduce the precursor and the solution was kept on

stirring for another 30 min to allow proper mixing resulting in a clear transparent solution. Later aqueous NH₃ was added dropwise till the pH of the solution became 8.5 and a milky white solution was obtained. The solution was kept on continuous stirring for another 3 h. After this the stirring was stopped and the beaker was kept undisturbed overnight in order to facilitate the particles to settle down completely.

The solution was then washed with DD water and ethanol multiple times so as to remove the residual chlorine content using 125 mm Whatman filter paper (Cat no. 1001 125). The resulting product was covered and left for drying overnight. The dried powder was then divided into three parts and annealed at 400 °C, 500 °C, and 600 °C named as Sn4, Sn5, and Sn6 respectively.

4 Characterization techniques

4.1 Sructure, morphology and elemental composition

To identify the crystalline structure and crystallite size of the prepared NPs, XRD studies were carried out using X'Pert PRO Wide Angle X-Ray Diffraction (WAXD) using Cu-kα source with voltage 40 kV and current 30 mA in the 2θ range 20° to 90° at a scan speed of 2°/min. The obtained XRD pattern of Sn4, Sn5 and Sn6 is shown in Fig. 1. We can observe a consistent narrowing of the peaks as the annealing temperature was increased which reflects upon the decreasing full width at half maxima (FWHM) as we go from Sn4 to Sn6. The narrowing of peaks is directly related to the increase in average crystallite size of the NPs. With
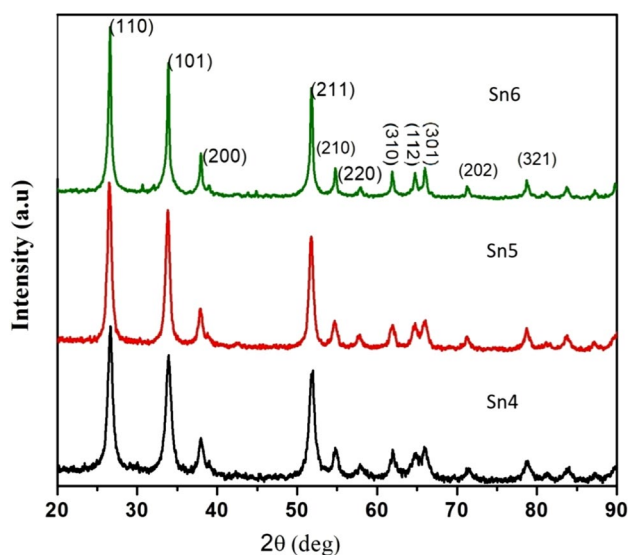

Fig. 1 XRD pattern of the SnO₂ NPs

the increase in the annealing temperature, the SnO_2 particles have more energy at their disposal which allows the particles to coalescence together, thereby leading to formation of bigger particles [16]. The crystalline size or average size of SnO_2 NPs can be estimated by using Debye–Scherrer Formula as shown in Eq. (1).

$$D = \frac{(k * \lambda)}{\beta * Cos\theta} \tag{1}$$

where 'D' represents average crystallite size, 'k' is the shape factor having value 0.9, 'λ' is wavelength of Cu-kα radiation (1.54059 Å), 'β' indicates FWHM of the peak and 'θ' is Bragg's angle in degrees. The calculated average crystalline size of SnO_2 NPs Sn4, Sn5 and Sn6 is 11.8 nm, 16.6 nm, and 35.8 nm respectively. Figure 2 shows the graphical representation of average crystallite size with the annealing temperature. The nonlinear increment in crystallite size with rise in annealing temperature is consistent with the available literature [17, 18].

The obtained XRD pattern corresponds to the tetragonal (rutile) phase of the SnO_2 crystal structure as confirmed by the JCPDS data 41-1445 and 88-0287 [14, 19]. Table 1 summarizes the major peak position (2θ), the d-spacing that represents interplanar distance, miller indices, and FWHM of the three samples. It can be clearly seen that the FWHM decreases from Sn4 to Sn6 with an almost consistent d-spacing. Further, it can be observed that some small peaks are also present in all the three samples which represent different miller indices of the tetragonal phase of SnO_2, however they tend to diminish in intensity with increase in average crystallite size. The absence of any overlapping peaks over the standard peaks confirms that
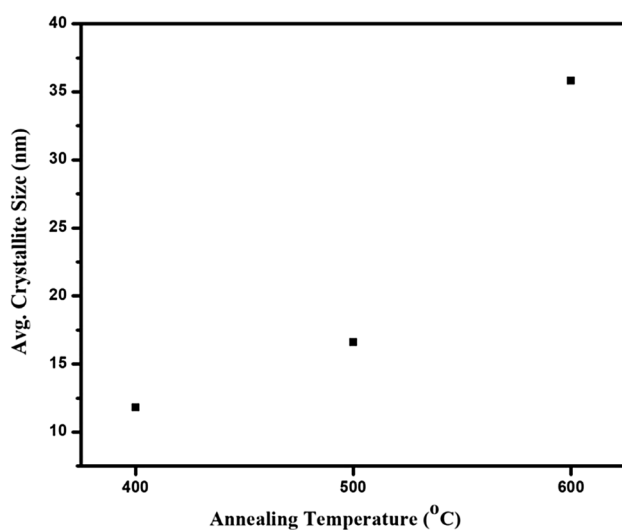
Table 1 XRD parameters of the SnO_2 NPs

Samples	Planes (hkl)	2θ (degrees)	FWHM (degrees)		d-spacing (Å)
Sn4	110	26.5900	0.70000	3.34964	
	101	33.8900	0.81000	2.64296	
	211	51.7975	0.75500	1.76358	
Sn5	110	26.5080	0.62400	3.35982	
	101	33.7814	0.63710	2.65121	
	211	51.7062	0.62750	1.76648	
Sn6	110	26.5556	0.33130	3.35390	
	101	33.8490	0.28250	2.64607	
	211	51.7620	0.28040	1.76471	

the prepared NPs have single phase and are devoid of any impurities.

ZEISS EVO 50 SEM with an acceleration voltage of 15 kV and a magnification of 4 k X was used to check the surface morphology of the SnO_2NPs. The powdered sample was spread uniformly on the conductive double-sided adhesive carbon tape (Micro to Nano, Product No. 15-000505). The obtained images are shown in Fig. 3. From the images it is clear that Sn4 (Fig. 3a) has almost circular shaped particles along with some non-uniform rod like structures and agglomerations. The non-uniformity in structure and agglomerations tend to increase in Sn5 and Sn6 (Fig. 3b, c). Owing to the increase in annealing temperature, the agglomerations in NPs occur leading to irregular morphology of the samples. As suggested by XRD, it is clearly observable through SEM that the average particle size has also increased from Sn4 to Sn6.

For assessing the elemental composition of the samples, RONTEC's EDX system Model QuanTax 200 attached to the SEM instrument was used. The obtained figures for the three samples are shown in Fig. 4. Table 2 shows the weight % and the atomic % of the corresponding elements as obtained from Fig. 4. From the analysis it is clear that Sn and O peaks are present in majority in the appropriate ratio thereby confirming the formation of SnO_2 NPs. Further trace peaks of C and Al can also be observed which are present due to the carbon tape that was used for the spreading of sample.

5 Optical study

5.1 UV–visible spectroscopy

Shimadzu 1800 UV–Vis spectrophotometer in the wavelength range of 200 nm to 800 nm was used to study the optical property of SnO_2 NPs. Small amount of the samples Sn4, Sn5 and Sn6 were taken in sample vials with DD

Fig. 2 Variation of average crystallite size with annealing temperature

**Fig. 3** SEM images of **a** Sn4, **b** Sn5, and **c** Sn6
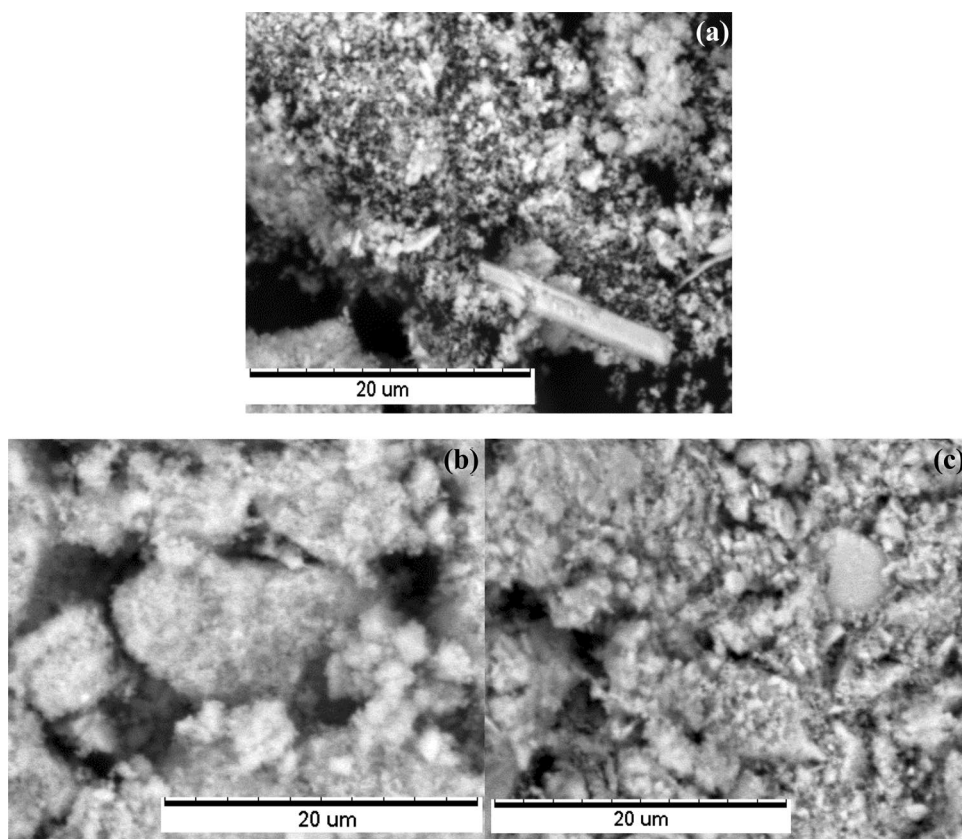
water and sonicated for 1 h so as to allow proper dispersion in the solvent. Few mL of sample was transferred to the quartz cuvette and dispersed in DD water for carrying out the analysis. The obtained absorption spectrum of Sn4, Sn5 and Sn6 NPs is shown in Fig. 5. The first absorption maxima (λ_{max}) of Sn4, Sn5 and Sn6 is observed at 289 nm, 292 nm and 303 nm respectively. A secondary absorption peak can also be seen at ~230 nm which is consistent for all the three samples. The samples show a consistent rise right from 800 to ~400 nm after which change in slope is observed. This kind of behavior is typical with wide bandgap semiconductors since they show no absorption in the visible region [20].

The optical bandgap energy (E_g) was calculated by using Tauc's relation a given in Eq. (2).

$$(\alpha h v) = A(h v - Eg)^{n/2} \qquad (2)$$

where 'α' is optical absorption coefficient, 'h' is planck's constant, 'v' is frequency of incident photon, 'hv' is energy of incident photon, 'E_g' is energy of optical bandgap. The plot $(\alpha hv)^2$ versus (hv) is obtained from it. Since the thickness of the sample is negligible in case of liquid medium, the value of 'α' is considered to be the same as that of Absorbance (A) which is obtained from the UV–Vis absorption. The value of optical band gap can be measured by

extrapolating a straight line from the plot to intersect the horizontal photon energy axis (absorption equal to 0). As mentioned previously that SnO_2 can possess both direct or indirect bandgap, however in our case it is direct bandgap as the indirect transition did not result in any 'straight line' which could be justified and extrapolated for evaluating the value of bandgap. From Fig. 6 it is observed that the optical bandgap energy of the nanoparticles does not follow the usual pattern of decrease in band gap with increase in the annealing temperature. The E_g of Sn4, Sn5 and Sn6 is found to be 3.5 eV, 3.7 eV, and 3.0 eV respectively. Compared to the direct bulk bandgap of SnO_2 (~3.68 eV), as the annealing temperature increases the bandgap of NPs is found to decrease as well as increase. This happens due to the fact that SnO_2 NPs do not follow quantum confinement effect strictly owing to the presence of defect sites in the crystal lattice and oxygen vacancies [21, 22]. The electronic structure of SnO_2 has a complex architecture thus its bandgap never follows any defined pattern [23]. Owing to this, we can see that the bandgap of Sn5 has increased to 3.7 eV before decreasing to 3.0 eV in Sn6. This irregular change in bandgap can easily be correlated with the elemental stoichiometry obtained from the EDX analysis (Table 2). The O:Sn ratio in Sn5 is least compared to Sn4 and Sn6, hence we have obtained a deviation in bandgap of SnO_2 NPs.

Fig. 4 EDX images of **a** Sn4, **b** Sn5, and **c** Sn6
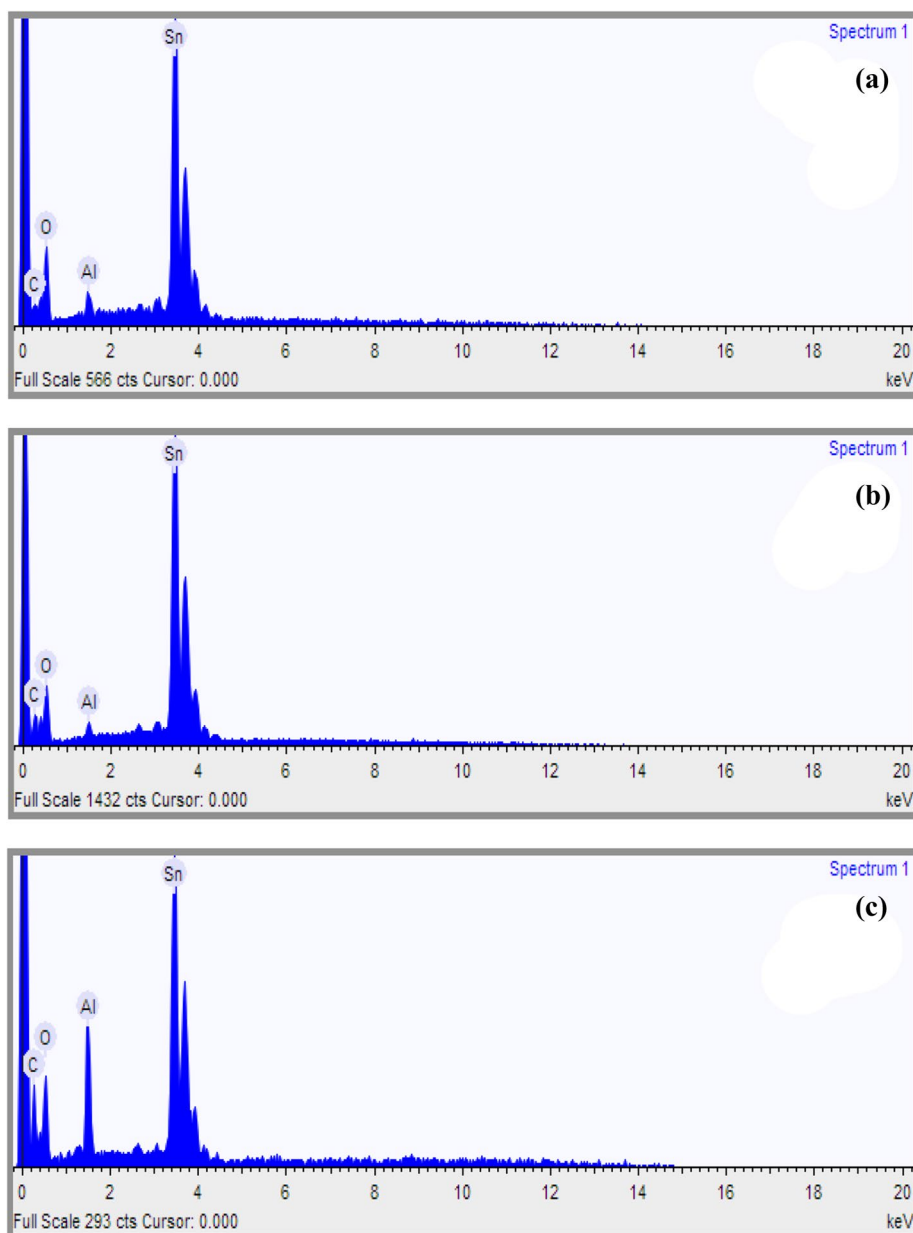
Table 2 Elemental composition of Sn4, Sn5 and Sn6

Element	Sn4		Sn5		Sn6	
	Weight (%)	Atomic (%)	Weight (%)	Atomic (%)	Weight (%)	Atomic (%)
Carbon	3.914	11.456	5.761	18.259	12.770	30.839
Oxygen	30.971	68.053	24.586	58.499	27.348	49.581
Aluminum	1.196	1.558	0.827	1.167	5.955	6.401
Tin	63.919	18.933	68.826	22.075	53.927	13.179

6 FTIR

The FTIR analysis of the SnO_2 NPs was carried out using Agilent CARY 630 in the wavelength range 400–4000 cm^{-1} to identify the functional groups and confirm the formation of SnO_2. Small amount of the NPs were sonicated in ethanol for an hour and 50 μL was dropped on the FTIR tip for analysis. The obtained spectrum is shown in Fig. 7. The broad peaks between 500
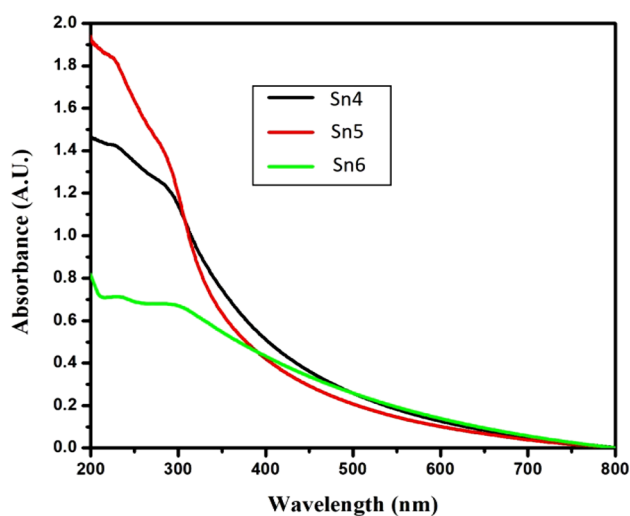
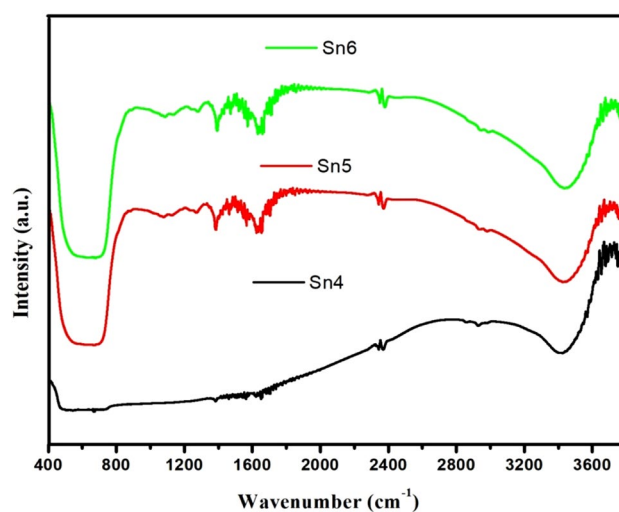**Fig. 5** UV–Vis Absorption spectra of Sn4, Sn5 and Sn6
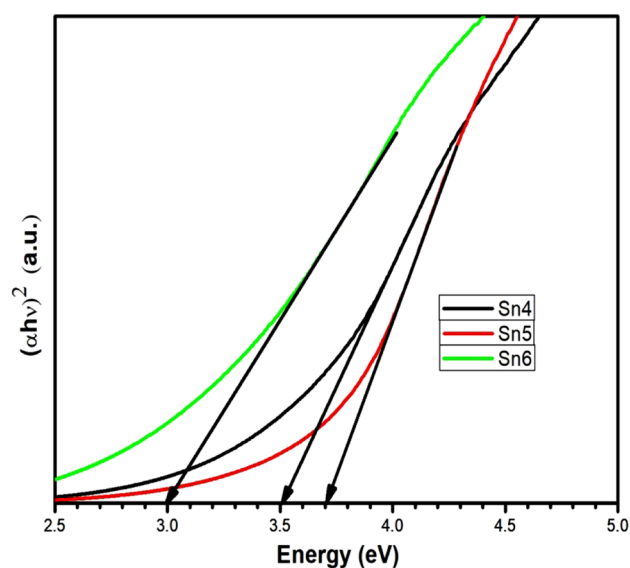

Fig. 7 FTIR spectra of Sn4, Sn5, Sn6

Fig. 6 Bandgap plot of Sn4, Sn5 and Sn6

and 700 cm^{-1} indicates the formation of SnO_2 [24, 25]. The rest of the peaks pertaining to C–H and O–H are due to the presence of ethanol thereby further confirming the purity of the prepared NPs. The obtained peaks are listed in Table 3.

7 Conclusion

In this paper we have successfully synthesized crystalline SnO_2 NPs via chemical co-precipitation method. Since chemical co-precipitation method does not require any high-end instruments for synthesis and the method itself is free from any complications, hence the synthesized SnO_2 NPs are low-cost and simple to reproduce. The XRD pattern revealed the tetragonal structure of the NPs with rutile phase. The average crystallite size of the NPs increased with increase in the annealing temperature while the optical bandgap energy showed deviation from the quantum confinement principle. SnO_2 being a compound with complex electronic structure, the bandgap did not show any patterned change with annealing temperature. SEM revealed the agglomeration and non-uniform nature of the particles with increase in the annealing temperature which is consistent with our previous observations. The EDX analysis confirmed the preparation of SnO_2 devoid of any impurities which was further affirmed with FTIR spectrum also. The chosen synthesis method is easily replicable for mass production of SnO_2 NPs. Further, the small crystallite size of the SnO_2 particles and the absence of any inherent impurities make it an excellent candidate for gas sensing purposes [26–28]. The prepared NPs are currently being tested for gas sensing applications and the results will be communicated shortly.

Table 3 Functional group identifications from FTIR spectrum

Sn4		Sn5		Sn6	
Wavenumber (cm^{-1})	Functional group	Wavenumber (cm^{-1})	Functional group	Wavenumber (cm^{-1})	Functional group
3414.48	O–H	3426.47	O–H	3414.48	O–H
2934.69	C–H stretch	2996.66	C–H stretch	2996.66	C–H stretch
2873.72	C–H stretch	2934.69	C–H stretch	2934.69	C–H stretch
1374.38	C–H rock	1374.38	C–H rock	1374.38	C–H rock
686.69	Sn–O–Sn	625.72	Sn–O–Sn	625.38	Sn–O–Sn

Compliance with ethical standards

Conflict of interest The authors declare that they have no competing interests.

References

1. Feynman RP (1960) There's plenty of room at the bottom. California Institute of Technology, Engineering and Science magazine, Pasadena
2. Koshy J, Chandran A, Samuel S, George KC (2014) Optical properties of SnO$_2$ nanoparticles. AIP Conf Proc 1620(1):192–196
3. Nahirniak S, Dontsova T, Astrelin I (2017) Directional synthesis of SnO$_2$-based nanostructures for use in gas sensors. In: International conference on nanotechnology and nanomaterials. Springer, Cham, pp 233–245
4. Nahirniak SV, Dontsova TA, Chen Q (2018) Sensing properties of SnO$_2$-MWCNTs nanocomposites towards H2. Mol Cryst Liq Cryst 674(1):48–58
5. Chand P (2019) Effect of pH values on the structural, optical and electrical properties of SnO$_2$ nanostructures. Optik 181:768–778
6. Nadaf LI, Venkatesh KS (2016) Synthesis and characterization of tin oxide nanoparticles by co-precipitation method. Mater Sci 32:98–101
7. Naje AN, Norry AS, Suhail AM (2013) Preparation and characterization of SnO$_2$ nanoparticles. Int J Innov Res Sci Eng Technol 2(12):7068–7072
8. Razeghizadeh AR, Zalaghi L, Kazeminezhad I, Rafee V (2015) Effects of Sol concentration on the structural and optical properties of SnO$_2$ nanoparticle. arXiv preprint arXiv:abs/1502.00219
9. Diao GQ, Li H, Ivanenko I, Dontsova T, Astrelin I, Xie FY, Guo XZ (2019) Comparison of SnO$_2$-carbon nanotubes composite and the SnO$_2$-carbon black mixture as an anode for Li-ion batteries. In: IOP conference series: materials science and engineering, vol 474, no. 1. IOP Publishing, p 012022
10. Thakare KS, Patil SJ, Deshmukh SB, Borse RY, Ahire RR (2016) Preparation, characterization and gas sensing performance of pure SnO$_2$ thin films deposited using physical vapour deposition. J Tech Eng 4(2):102–116
11. Chiu HC, Yeh CS (2007) Hydrothermal synthesis of SnO$_2$ nanoparticles and their gas-sensing of alcohol. J Phys Chem C 111(20):7256–7259
12. Zhu JJ, Zhu JM, Liao XH, Fang JL, Zhou MG, Chen HY (2002) Rapid synthesis of nanocrystalline SnO$_2$ powders by microwave heating method. Mater Lett 53(1–2):12–19
13. Nehru LC, Sanjeeviraja C (2014) Rapid synthesis of nanocrystalline SnO$_2$ by a microwave-assisted combustsion method. J Adv Ceram 3(3):171–176
14. Chen W, Ghosh D, Chen S (2008) Large-scale electrochemical synthesis of SnO$_2$ nanoparticles. J Mater Sci 43(15):5291–5299
15. Choudhury SP, Kumari N, Bhattacharjee A (2014) Comparative X-ray diffraction study of SnO$_2$ nanoparticle samples from different precursor solutions. Cell 69:71–281
16. Gaber A, Abdel-Rahim MA, Abdel-Latief AY, Abdel-Salam MN (2014) Influence of calcination temperature on the structure and porosity of nanocrystalline SnO$_2$ synthesized by a conventional precipitation method. Int J Electrochem Sci 9(1):81–95
17. Zhou W, Liu Y, Yang Y, Wu P (2014) Band gap engineering of SnO$_2$ by epitaxial strain: experimental and theoretical investigations. J Phys Chem C 118(12):6448–6453
18. Kamble VB, Umarji AM (2013) Defect induced optical bandgap narrowing in undoped SnO$_2$ nanoparticles. AIP Adv 3(8):082120
19. Esmaeili-Bafghi-Karimabad A, Ghanbari D, Salavati-Niasari M, Nejati-Moghadam L, Gholamrezaei S (2015) Photo-catalyst tin dioxide: synthesis and characterization different morphologies of SnO$_2$ nanostructures and nanocomposites. J Mater Sci 26(9):6970–6978
20. Paul Raj S (2013) Mineralization of azo dye using combined photo-fenton and photocatalytic processes under visible light. J Catal
21. Babar AR, Shinde SS, Moholkar AV, Rajpure KY (2010) Electrical and dielectric properties of co-precipitated nanocrystalline tin oxide. J Alloy Compd 505(2):743–749
22. Jain K, Lakshmikumar ST (2005) Preparation of nanocrystalline tin oxide powder for gas sensor applications. J Surf Sci Technol 21(3–4):129–138
23. Batzill M, Diebold U (2005) The surface and materials science of tin oxide. Prog Surf Sci 79(2–4):47–154
24. Aziz M, Abbas SS, Baharom WRW, Mahmud WZW (2012) Structure of SnO$_2$ nanoparticles by sol–gel method. Mater Lett 74:62–64
25. Zinatloo-Ajabshir S, Morassaei MS, Salavati-Niasari M (2017) Facile fabrication of Dy$_2$Sn$_2$O$_7$-SnO$_2$ nanocomposites as an effective photocatalyst for degradation and removal of organic contaminants. J Colloid Interface Sci 497:298–308
26. Dieguez A, Romano-Rodriguez A, Morante JR, Weimar U, Schweizer-Berberich M, Göpel W (1996) Morphological analysis of nanocrystalline SnO$_2$ for gas sensor applications. Sens Actuators B 31(1–2):1–8
27. Choudhary M, Mishra VN, Dwivedi R (2014) Gas sensing properties of tin oxide nano-powder synthesized via sol–gel route. In: Physics of semiconductor devices. Springer, Cham, pp 621–624

28. Zhang G, Liu M (2000) Effect of particle size and dopant on properties of SnO2-based gas sensors. Sens Actuators B 69(1–2):144–152

Publisher's Note Springer Nature remains neutral with regard to jurisdictional claims in published maps and institutional affiliations.